Pergamon

0020-7225(95)00030-5

Int. J. Engng Sci. Vol. 33, No. 12, pp. 1699–1711, 1995

0020-7225/95 $9.50 + 0.00

THERMALLY DRIVEN FLOWS AT LOW PRANDTL NUMBERS: AN EXTENSION OF THE PRANDTL–BATCHELOR THEOREM

P. A. BLYTHE, A. LIAKOPOULOS and E. HARUTA†

Department of Mechanical Engineering and Mechanics, Packard Laboratory, 19 Memorial Drive West, Lehigh University, Bethlehem, PA 18015-3085, U.S.A.

(Communicated by D. G. B. EDELEN)

Abstract—New results for the structure of closed eddies in thermally driven flows at low Prandtl numbers and high Grashof numbers are presented. The analysis provides an extension of the classical Prandtl–Batchelor theorem. Numerical calculations given here for laterally heated rectangular cavities are in excellent agreement with the extended theorem.

1. INTRODUCTION

Steady two-dimensional flows with closed streamlines are characterized, at high Reynolds numbers Re, by a constant vorticity core (Prandtl [1], Batchelor [2]). This result, usually called the Prandtl–Batchelor theorem, is based on an exact integral constraint derived from the Navier–Stokes equations under the assumption that viscous effects ($\mathrm{Re} \gg 1$) are confined to a thin layer near some outer bounding (singular) streamline. In principle, the core vorticity is then determined by matching with the shear layer solution. Applications have been discussed, for example, by Smith [3] and by Moore *et al.* [4].

Extensions to thermally diffusive flows have been made by Weinbaum [5], Burggraf [6], and Grimshaw [7] for limits in which the Prandtl number is 0(1). In this case, an integral constraint can also be derived from the energy equation and, for two-dimensional flows, leads to the conclusion that the temperature is constant in the eddy core. This result, however, does require the existence of a central non-diffusive set of nested streamlines. Not all bounded flows involving thermal diffusion are of this type (Gill [8]).

Approaches that extend these classical results have been given by Read *et al.* [9] for vortex dynamics in certain geophysical problems, and by Mestel [10] for magnetohydrodynamic flows at low magnetic Reynolds numbers. In both cases, the two-dimensional Prandtl–Batchelor theorem takes the form

$$\frac{\mathrm{d}\zeta}{\mathrm{d}\psi} \propto \frac{\oint \mathbf{F} \cdot \mathrm{d}\mathbf{s}}{\oint \mathbf{v} \cdot \mathrm{d}\mathbf{s}} \tag{1.1}$$

where the line integrals are evaluated over a closed streamline, ζ is the vorticity, ψ is the streamfunction, $\mathbf{v}$ is the velocity, $\mathbf{F}$ is an appropriate body force per unit mass, and s denotes distance around the streamline. For zero (or a conservative) body force the right-hand side of (1.1) vanishes and the classical result $\zeta = \text{const.}$ is recovered.

The present paper is concerned with an analogous extension to thermal convection at low Prandtl numbers but large Grashof numbers Gr. For the low Prandtl number limit, (1.1) is replaced by

$$\frac{\mathrm{d}\zeta}{\mathrm{d}\psi} \propto \frac{\mathscr{A}}{K} \tag{1.2}$$

†Present address: IBM, Poughkeepsie, New York.

where $\mathscr{A}$ is the area inside the closed streamline and K is the circulation around it. Applications of the theory are given here for differentially heated square and rectangular cavities.

A suitable low Prandtl number formulation is outlined in Section 2. The derivation of (1.2) is discussed in Section 3. For the flows considered, the appropriate asymptotic limit is described by $\mathrm{Pr} = 0$, $\mathrm{Gr} \to \infty$. Numerical solutions of the governing partial differential equations ($\mathrm{Pr} = 0$) are presented in Section 4 for large but finite Grashof numbers. The numerical computations are carried out using a spectral element method, and the results provide good test cases for the extended Prandtl–Batchelor theorem (1.2). New analytical solutions based on (1.2) are determined for the special case of circular symmetry. These solutions are also exact solutions of the full partial differential equations ($\mathrm{Pr} = 0$), and are in excellent agreement with numerical solutions for square cavities (see Section 5). More general solutions, not involving circular symmetry, are considered in Section 6 where an analysis of the flow near the eddy center is given. Again the numerical and analytical solutions are in close agreement.

The results described in this paper provide firm support for the validity of the extended Prandtl–Batchelor theorem (1.2) when applied to high Grashof number flows at zero Prandtl number.

2. GOVERNING EQUATIONS

The flow domain is a rectangular cavity of length ℓ and height h. Appropriate co-ordinates are defined in Fig. 1. Steady two-dimensional flows are generated by maintaining the vertical cavity walls at fixed but different temperatures; the horizontal boundaries are adiabatic. In view of the subsequent high Grashof number limit, it is convenient to introduce dimensionless variables by setting

$$\left.\begin{aligned} \mathbf{v}' = (u', w') = \frac{\nu}{\ell}\mathrm{Gr}(u, w) = \frac{\nu}{\ell}\mathrm{Gr}\,\mathbf{v}, \\ T' - T'_{\mathrm{c}} = (T'_{\mathrm{H}} - T'_{\mathrm{c}})T, \qquad p' = \rho'_0 \frac{\nu^2}{\ell^2}\mathrm{Gr}^2 p, \\ (x', z') = \ell(x, z), \qquad t' = \frac{\ell^2}{\nu\,\mathrm{Gr}}t, \end{aligned}\right\} \tag{2.1}$$

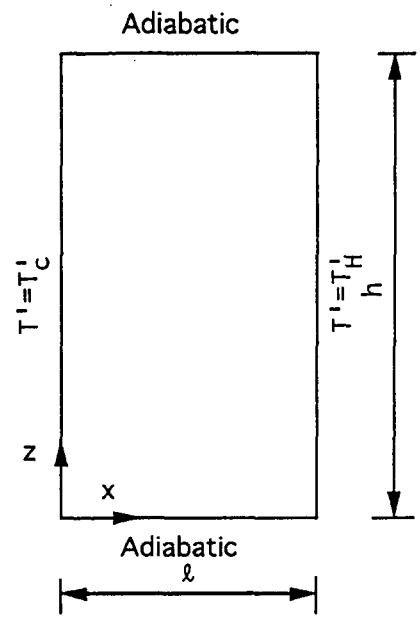

Fig. 1. Flow domain and thermal boundary conditions.

where primes denote dimensional values, ν is the kinematic viscosity, and the Grashof number

$$\mathrm{Gr} = \frac{g\beta(T'_{\mathrm{H}} - T'_{\mathrm{c}})\ell'^3}{\nu^2}. \tag{2.2}$$

Here g is the acceleration due to gravity, and β is the volumetric expansion coefficient. Also $(T'_{\mathrm{H}} - T'_{\mathrm{c}})$ is the temperature difference between the hot and cold walls, ρ'_0 is the background density, and the local pressure p' is measured from its background hydrostatic value. In (2.1), T' is the temperature, v' is the velocity, and t' denotes time.

Invoking the Boussinesq approximation, the governing dimensionless equations become

$$\nabla \cdot \mathbf{v} = 0, \tag{2.3}$$

$$\mathrm{Gr}\left(\frac{\mathrm{D}\mathbf{v}}{\mathrm{D}t} + \nabla p\right) = \nabla^2 \mathbf{v} + \mathbf{k}T, \tag{2.4}$$

$$\mathrm{Pr}\,\mathrm{Gr}\frac{\mathrm{D}T}{\mathrm{D}t} = \nabla^2 T, \tag{2.5}$$

where $\mathrm{Pr}(=\nu/\kappa)$ is the Prandtl number, κ is the thermal diffusivity, and $\mathbf{k}$ is the unit vector in the z-direction. Corresponding boundary conditions are

$$\left.\begin{aligned} &\mathbf{v} = \mathbf{0} \quad \text{on} \quad x = 0, 1, \\ &T = 0 \quad \text{on} \quad x = 0, \qquad T = 1 \quad \text{on} \quad x = 1, \end{aligned}\right\} \tag{2.6a}$$

and

$$\mathbf{v} = \mathbf{0}, \qquad \frac{\partial T}{\partial z} = 0 \quad \text{on} \quad z = 0, A \tag{2.6b}$$

where $A = h/\ell$ is the cavity aspect ratio.

At zero Prandtl number, the temperature distribution

$$T = x \tag{2.7}$$

and, using (2.4), the vorticity equation can be written

$$\mathrm{Gr}\frac{\mathrm{D}\zeta}{\mathrm{D}t} = \nabla^2 \zeta - 1 \tag{2.8}$$

with

$$\boldsymbol{\zeta} = \nabla \times \mathbf{v} = (0, \zeta, 0) = (0, \nabla^2 \psi, 0). \tag{2.9}$$

The stream function ψ is defined by

$$u = \frac{\partial \psi}{\partial z}, \qquad w = -\frac{\partial \psi}{\partial x}. \tag{2.10}$$

As usual, for a steady (time-independent) state, it follows from (2.8) that in the non-diffusive limit ($\mathrm{Gr} \gg 1$)

$$\zeta = f(\psi). \tag{2.11}$$

In this limit it is also convenient, following Batchelor [2], to re-write the momentum equation (2.4) in the form

$$\mathrm{Gr}\left(\nabla H + \frac{\partial \mathbf{v}}{\partial t} - \mathbf{v} \times \boldsymbol{\zeta}\right) = \mathbf{k}x + \nabla \times \boldsymbol{\zeta} \tag{2.12}$$

where

$$H = p + \frac{1}{2}v^2. \tag{2.13}$$

3. FLOWS WITH CLOSED STREAMLINES

For time-independent flows, integration of (2.12) around a closed streamline yields

$$\oint (\nabla \times \boldsymbol{\zeta}) \cdot \mathrm{d}\mathbf{s} = \oint x\mathbf{k} \cdot \mathrm{d}\mathbf{s} \tag{3.1}$$

where s measures distance along the streamline. In the non-diffusive limit (2.12) implies that

$$\nabla H = \mathbf{v} \times \boldsymbol{\zeta}. \tag{3.2}$$

Consequently, for the two-dimensional flows considered here, it follows that $H = H(\psi)$ with

$$\zeta = \frac{\mathrm{d}H}{\mathrm{d}\psi} \tag{3.3}$$

which is consistent with (2.11). Substitution of this limiting behavior ($\mathrm{Gr} \gg 1$) into the exact result (3.1) gives

$$\frac{\mathrm{d}\zeta}{\mathrm{d}\psi} = -\frac{\oint x\mathbf{k} \cdot \mathrm{d}\mathbf{s}}{\oint \mathbf{v} \cdot \mathrm{d}\mathbf{s}} = -\frac{\mathscr{A}}{K} \tag{3.4}$$

where $\mathscr{A}$ is the area enclosed by the streamline, and K is the circulation around the streamline.

The classical Prandtl–Batchelor theorem [1, 2] corresponds to the case when there is no body force, and the right-hand side of (3.4) then vanishes implying that the vorticity is constant inside a closed streamline. As in the classical problem, it is assumed in deriving (3.4) that the streamlines do not pass through any boundary region where diffusive effects cannot be neglected. Vorticity generation in surrounding shear layers, etc. must be considered before the complete internal structure defined by (3.4) can be found (Sections 5 and 6).

Extensions of the Prandtl–Batchelor theorem to cases in which the body force is significant have previously been discussed by Read *et al.* [9], and by Mestel [10]. The present extension for the low Prandtl number limit is particularly simple and specific solutions are developed in Sections 5 and 6.

4. NUMERICAL SOLUTIONS

The governing equations (2.3)–(2.5) were solved, subject to (2.6), using a spectral element method (Patera [11]). Nekton [12] is a particular implementation of this method that is well suited to direct numerical studies of temporal thermofluid instabilities. Asymptotically steady solutions, obtained from Nekton in the limit $t \to \infty$, have been compared with solutions determined by a steady Navier–Stokes spectral solver (Liakopoulos [13]). For the range of

Grashof numbers considered here, the asymptotic and steady solutions are in excellent agreement. Since it is necessary to compute steady solutions for $Gr \gg 1$, it is important to safeguard against calculating solutions that are not physically realizable, i.e. that are unstable with respect to small perturbations. All results discussed in this paper correspond to time accurate solutions of the unsteady equations. Although this approach is computationally intensive, because of the existence of long transients when $Gr \gg 1$, it does lead to unique time-independent solutions provided that Gr is not too large. Because of the presence of geometric singularities at the corners of the computational domain, the "noise" level is sufficiently high to trigger any temporal instabilities. The stability of the computed flow fields was also checked by superimposing random initial disturbances and following their time evolution. Over the range of parameter values considered in the present paper, all such perturbations decayed as $t \to \infty$. Consequently, the solutions are stable to small perturbations and, with a high degree of confidence, can be classified as asymptotically time-independent.

Calculations were made over a range of Grashof numbers ($\leq 10^6$) at two particular aspect ratios $A = 1$ and 2. Corresponding spectral meshes are shown in Fig. 2. Within each element the order of approximation N was made sufficiently high so that spatial convergence (grid independence) was achieved. At low Gr this required $N = 5$; for higher values ($Gr \geq 10^5$) up to $N = 13$ was used.

Computational results are displayed in Fig. 3 for $A = 1$ and $Gr = 10^6$, and in Fig. 4 for $A = 2$ and $Gr = 5 \times 10^4$. In the case of a square cavity the streamlines are approximately circular [see Fig. 3(a)], and it is clear from Figs 3(a) and (b) that the type of law implied by (2.11) and (3.3), i.e. $\zeta = \zeta(\psi)$ and $H = H(\psi)$, is valid over most of the flow domain. When $A = 2$ the streamlines in the center of the cavity are roughly elliptic [see Fig. 4(a)], as are the isovorticity lines. It is apparent, however, that $\zeta = \zeta(\psi)$ has a much more restricted range of validity. At

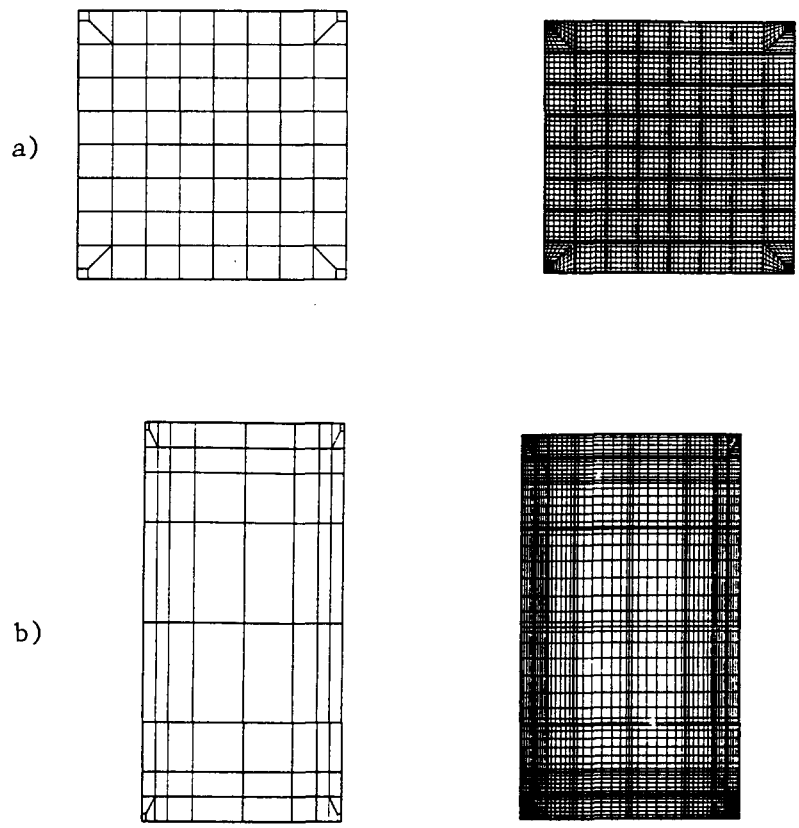

Fig. 2. Spectral element meshes and collocation points (for $N = 9$). (a) $A = 1$, (b) $A = 2$.

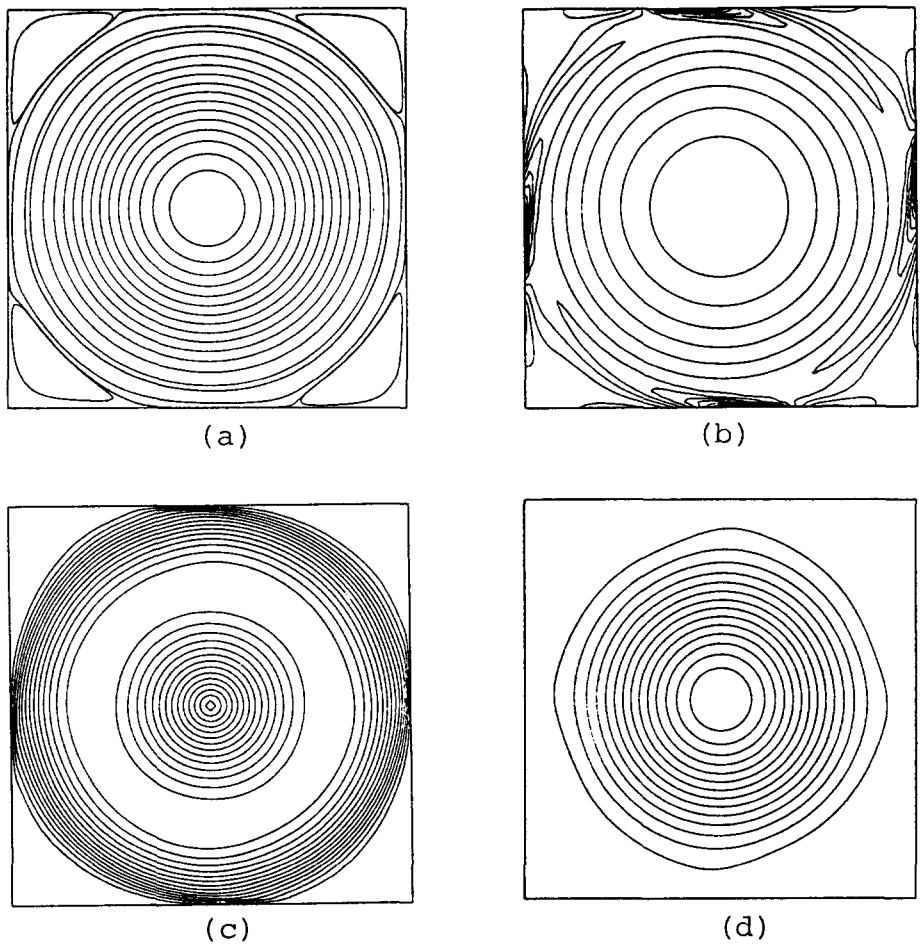

Fig. 3. $A = 1$, $\mathrm{Gr} = 10^6$. (a) Streamlines, (b) iso-vorticity lines, (c) constant-speed contours, (d) isobars. For this figure, in contrast with the formulation of Section 2, the hot wall is at $x = 0$ and the cold wall is at $x = 1$, thus generating a clockwise main circulation. The solution is centro-symmetric [8]. The weak secondary cells at the corners are made visible by selecting unequally spaced streamfunction contours.

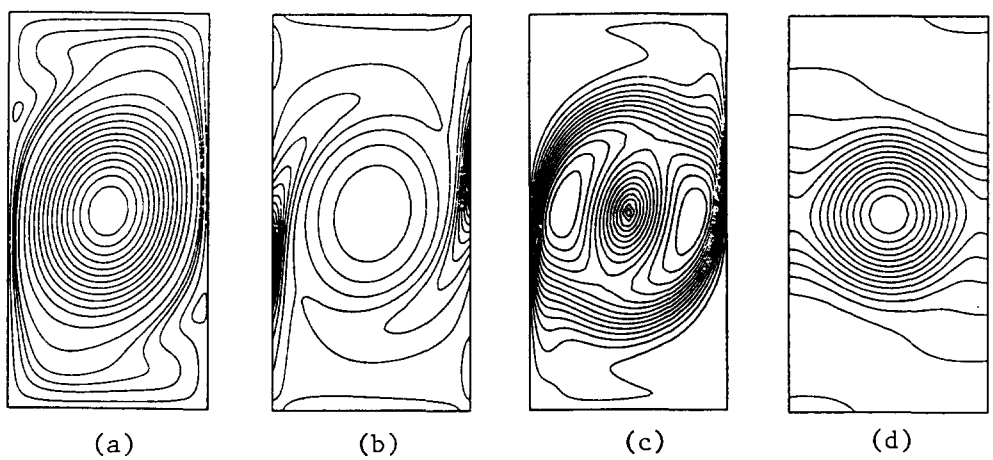

Fig. 4. $A = 2$, $\mathrm{Gr} = 5 \times 10^4$. (a) Streamlines, (b) iso-vorticity lines, (c) constant-speed contours, (d) isobars. For this figure, in contrast with the formulation of Section 2, the hot wall is at $x = 0$ and the cold wall is at $x = 1$, thus generating a clockwise main circulation. The solution is centro-symmetric [8]. Unequally spaced streamfunction contours are selected to depict the flow structure close to the corners.

$Gr = 5 \times 10^4$, $A = 2$, diffusive layers near the cavity boundaries obviously exert a stronger influence on the overall flow structure. For all cases the steady solutions are centro-symmetric, Gill [8].

A discussion of the circular streamline case is given in Section 5 where solutions derived from the modified Prandtl–Batchelor law (3.4) are obtained and contrasted with the numerical results depicted in Fig. 3. Local solutions of (3.4), valid near the eddy center, are discussed for general values of A in Section 6. A comparison with the computational results for $A = 2$ is made there.

5. CIRCULAR STREAMLINES

At high Grashof numbers, when $Pr = 0$, the core streamlines in square cavities are approximately circular (see Fig. 3). For this case closed form solutions of (3.4) can be obtained. Ignoring the corner region, $\psi = \psi(r)$ decreases monotonically from its maximum value at the cavity center $r = 0$. Consequently, the speed

$$q = \left|\frac{d\psi}{dr}\right| = -\frac{d\psi}{dr} \tag{5.1}$$

where the radial co-ordinate r is made dimensionless with respect to the cavity length ℓ. Note that in the circular case the speed is constant on a streamline. Also, from (3.4),

$$\frac{d\zeta}{d\psi} = -\frac{r}{2q} = \frac{r}{2}\frac{dr}{d\psi}$$

and hence

$$\zeta = -\omega + \frac{r^2}{4} \tag{5.2}$$

where $-\omega$ is the vorticity at the eddy center. Since

$$\zeta = \nabla^2\psi = \frac{d^2\psi}{dr^2} + \frac{1}{r}\frac{d\psi}{dr}$$

it follows from (5.2) that

$$\psi = \psi_m - \frac{\omega r^2}{4} + \frac{r^4}{64} \tag{5.3}$$

where $\psi_m = \psi(0)$. Alternatively, again using (5.2),

$$\zeta = \omega - 2\sqrt{\omega^2 - (\psi_m - \psi)}. \tag{5.4}$$

The above analysis provides no information on either ω or ψ_m. In general, these quantities are defined through matching with local solutions valid near the cavity walls. Assuming that the volume flux through these inner layers is relatively small suggests that

$$\psi\left(\frac{1}{2}\right) = 0 \tag{5.5}$$

so that

$$\psi_m = \frac{1}{16}\left(\omega - \frac{1}{64}\right). \tag{5.6}$$

Table 1. Numerical and analytical values of ψ_m

Gr	ω	$(\psi_m)_{\text{num}}$	$(\psi_m)_{(5.6)}$
10^5	0.0345	0.001197	0.001180
5×10^5	0.0335	0.001125	0.001117
10^6	0.0331	0.001099	0.001096

Comparison with the numerical calculations is shown in Table 1. Note that both values of ψ_m are based on the numerically determined values of ω. Over the range $10^5 \leq \text{Gr} \leq 10^6$ the discrepancy between (5.6) and the numerical solutions is less than 1.5%.

In fact, (5.3) is an exact solution of the vorticity equation (2.8) and it seems reasonable to assume that

$$q\left(\frac{1}{2}\right) = 0. \tag{5.7}$$

Consequently, from (5.3) and (5.6),

$$\omega = \omega_\infty = 2^{-5}, \qquad \psi_m = \psi_\infty = 2^{-10}, \tag{5.8}$$

where the subscript ∞ is used to denote theoretical limiting values as $\text{Gr}\to\infty$. The result (5.8) implies

$$\psi_\infty = \omega_\infty^2 \tag{5.9}$$

so that (5.4) becomes

$$\zeta = \omega_\infty - 2\sqrt{\psi}, \tag{5.10}$$

and the slope $\mathrm{d}\zeta/\mathrm{d}\psi$ is singular on the boundary $\psi = 0$. Table 2 shows a test of the relation (5.9) based on the numerically determined values of ψ_m and ω at large finite Grashof numbers.

As can be seen from the table, (5.9) does appear to describe the limiting behavior as $\text{Gr}\to\infty$. There are, however, much larger discrepancies between the numerical and limiting values for the individual quantities ψ_m and ω. Least squares fits to the numerical data suggest that

$$\begin{aligned} \psi_m &= \psi_\infty + 0.00391\,\text{Gr}^{-0.25} + \ldots, \\ \omega &= \omega_\infty + 0.0625\,\text{Gr}^{-0.25} + \ldots, \end{aligned} \tag{5.11a}$$

which can be approximated by

$$\begin{aligned} \psi_m &= \psi_\infty + 2^{-8}\,\text{Gr}^{-1/4} + \ldots, \\ \omega &= \omega_\infty + 2^{-4}\,\text{Gr}^{-1/4} + \ldots, \end{aligned} \tag{5.11b}$$

so that

$$\psi_m - \omega^2 = o(\text{Gr}^{-1/4}). \tag{5.12}$$

Table 2. The hypothesis (5.7)

Gr	$\left\lvert\frac{\psi_m - \omega^2}{\psi_m}\right\rvert$
10^5	0.005
5×10^5	0.003
10^6	$<10^{-3}$

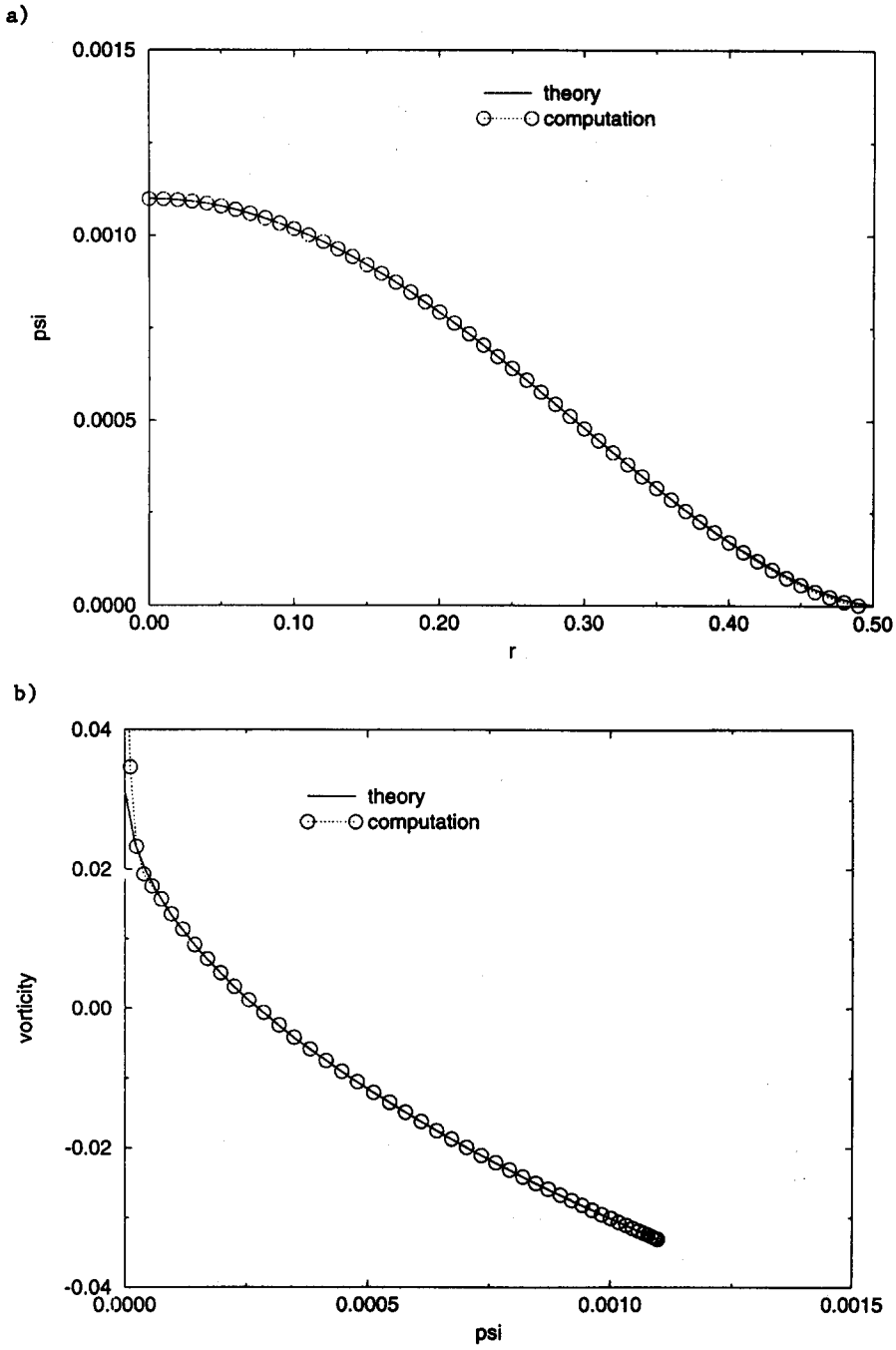

Fig. 5. (a) Comparison of theoretical streamfunction distribution $\psi = \psi(r)$, see (5.3), with numerical results. $A = 1$, $\mathrm{Gr} = 10^6$; (b) comparison of theoretical vorticity distribution $\zeta = \zeta(\psi)$, see (5.4), with numerical results. $A = 1$, $\mathrm{Gr} = 10^6$.

This confirms the behavior suggested by Table 2, i.e. the magnitude of $(\psi_m - \omega^2)/\psi_m$ is small in comparison with the relative differences in $\psi_m - \psi_\infty$ and $\omega - \omega_\infty$.

Nevertheless, the stream function variation given by (5.3), with ψ_m and ω defined by the numerical values listed in Table 1, is in excellent agreement with the computational results [see Fig. 5(a)]. Comparison with the numerical calculations for the vorticity law (5.4) is shown in Fig. 5(b). Remarkable agreement is again obtained. In addition, the theoretical speed

$$q = -\frac{\mathrm{d}\psi}{\mathrm{d}r} = \frac{\omega r}{2} - \frac{r^3}{16} \tag{5.13}$$

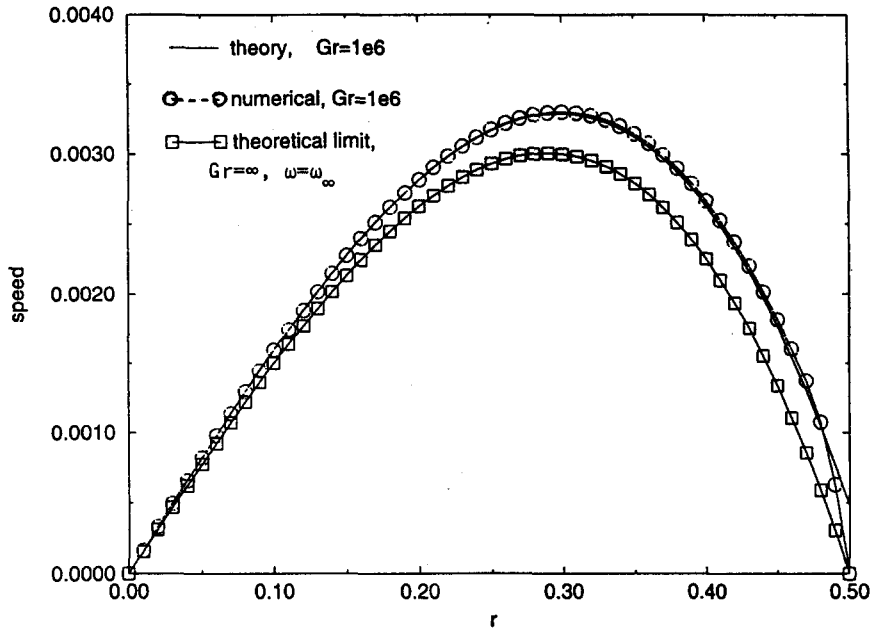

Fig. 6. Comparison of theoretical speed variation with numerical results.

is also consistent with the numerical data (see Fig. 6). As can be seen from (5.10), the velocity profile is predicted to have a maximum at

$$r = \sqrt{\frac{8\omega}{3}} < \frac{1}{2}, \tag{5.14}$$

which is very close to the location determined by the numerical solution. The limiting curve as $\mathrm{Gr} \to \infty$ is also shown in Fig. 6.

6. NON-CIRCULAR STREAMLINES: CORE STRUCTURE

For the circular case, the integration of (3.4) is straightforward and, as noted in Section 5, corresponds to an exact solution of the full vorticity equation (2.8). In the non-circular case, closed form representations for the global solution are not easily obtained. The structure of the solution near the eddy center can, however, be found without imposing any direct restrictions on the eddy shape.

If the vorticity at the eddy center, where $\psi = \psi_m$, is again denoted by $-\omega$, then

$$\zeta \sim -\omega + a_1(\psi_m - \psi) + \ldots \tag{6.1}$$

as $\psi \to \psi_m$. Consequently, from (3.4) using polar co-ordinates (r, θ) with origin at the eddy center,

$$\frac{\mathscr{A}}{K} \to a_1 \qquad \text{as } r \to 0. \tag{6.2}$$

Assuming regularity at the eddy center requires

$$\psi \sim \psi_m + b_2(\theta) r^2 + \ldots \tag{6.3}$$

as $r \to 0$. From (2.9) it can be established that

$$b_2(\theta) = \gamma_2 \cos[2(\theta - \delta)] - \frac{\omega}{4} \tag{6.4}$$

where the amplitude γ_2 and the phase δ are arbitrary constants. By suitably defining δ it is permissible to view $\gamma_2 > 0$ with

$$\frac{\omega}{4} > \gamma_2 > 0. \tag{6.5}$$

In addition, it is convenient to introduce the notation

$$\frac{\omega}{4} = c(1+\lambda^2), \qquad \gamma_2 = c(1-\lambda^2), \qquad \text{with } 0 < \lambda < 1, \tag{6.6}$$

where c is a positive constant. From (6.3) the local streamline shape is given by

$$\frac{\psi_m - \psi}{c} = r^2[1 + \lambda^2 - (1-\lambda^2)\cos 2\theta] \tag{6.7}$$

where, for notational simplicity, θ is measured relative to δ. Clearly, to leading order, the streamlines defined by (6.7) are elliptic with an aspect ratio λ. The parameter δ represents the tilt of the ellipse with respect to the original Cartesian co-ordinates. ($\theta = 0$ now defines the semi-major axis.)

Straightforward calculations yield

$$\frac{q}{c} = 2\sqrt{2}\, r[1 + \lambda^4 - (1-\lambda^4)\cos 2\theta]^{1/2} \tag{6.8}$$

and the circulation

$$K = 8(\psi_m - \psi)\int_0^{\pi/2} \frac{[1-(1-\lambda^4)\sin^2\phi]^{1/2}}{1-(1-\lambda^2)\sin^2\phi}\,\mathrm{d}\phi = 8(\psi_m - \psi)I(\lambda). \tag{6.9}$$

The latter result can be re-expressed in terms of elliptic integrals of the first and third kind. From (6.2) it now follows that, at the eddy center,

$$\frac{\mathrm{d}\zeta}{\mathrm{d}\psi} = -a_1 = -g(\lambda)\frac{1}{\omega} \tag{6.10}$$

where

$$g(\lambda) = \frac{\pi(1+\lambda^2)}{4\lambda I(\lambda)}. \tag{6.11}$$

For $1 \geq \lambda \gtrsim 0.6$ the function g is only weakly dependent on the aspect ratio λ (see Fig. 7). At $\lambda = 1$, $g(\lambda) = 1$ and the result (6.10) reduces to that for the circular case.

Computational results for $A = 2$ were discussed in Section 4. Local numerical data for the region near the eddy center suggest that $\lambda \approx 0.78$, and also

$$\frac{\mathrm{d}\zeta}{\mathrm{d}\psi} \approx -\frac{1.0}{\omega}, \tag{6.12}$$

whereas the calculations based on (6.10), with $\lambda = 0.78$, give

$$\frac{\mathrm{d}\zeta}{\mathrm{d}\psi} = -\frac{1.015\ldots}{\omega}. \tag{6.13}$$

This agreement is remarkably good since the accuracy of the numerical calculations for the derivative $\mathrm{d}\zeta/\mathrm{d}\psi$ at the eddy center is not particularly high. (The full partial differential equations are solved in terms of the primitive variables u, w, p and T.) In contrast, the local velocity distribution along a streamline should be accurately predicted by the numerical

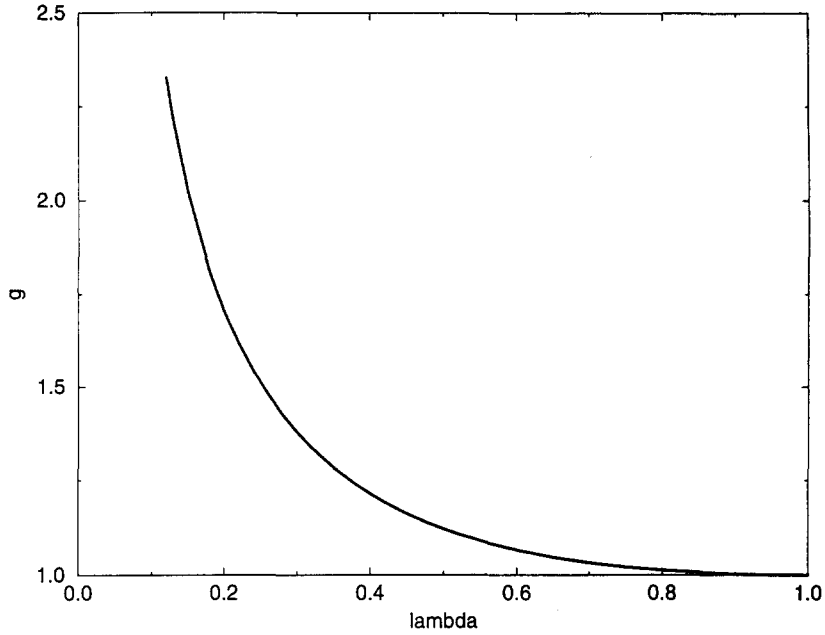

Fig. 7. The function $g(\lambda)$, see (6.11).

scheme. A comparison with the present theory (see 6.8) is shown in Fig. 8 and excellent agreement is indeed found.

7. CONCLUDING REMARKS

The extension (3.4) of the Prandtl–Batchelor theorem to low Prandtl number convective flows has been tested by direct numerical simulation for square and rectangular cavities. In the square case, the core streamlines are approximately circular and an exact solution of (3.4) exists. Excellent agreement between the numerical calculations and the analysis is obtained.

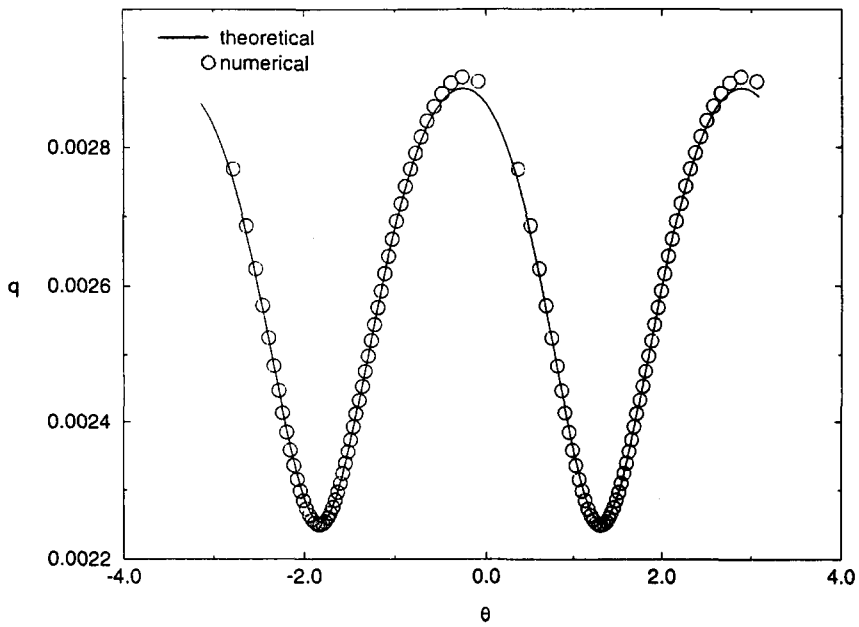

Fig. 8. Speed variation along a streamline $|\psi| = 1.78 \times 10^{-3}$. $A = 2$, $\mathrm{Gr} = 5 \times 10^4$.

For circular streamlines the solution of (3.4) corresponds to an exact solution of the full vorticity equation (2.8). This is also a property of the classical Prandtl–Batchelor result (no body force) which leads to $\zeta = \text{const.}$ irrespective of the shape of the closed streamlines. Hence, it is of interest to ask whether exact solutions $\zeta = \zeta(\psi)$ exist for the present class of problems, with body force, that are defined by (2.8). Although this is true for circular streamlines, requiring it to be true in general implies that

$$\zeta \frac{d\zeta}{d\psi} + q^2 \frac{d^2\zeta}{d\psi^2} = 1 \tag{7.1}$$

and hence $q = q(\psi)$. As noted above, the latter statement does hold for circular streamlines but is demonstrably not correct for the local solution defined by (6.8) and for the related numerical solutions discussed in Section 4, see Fig. 8. Proper application of the law (3.4) does, however, give excellent agreement with numerical calculations for cavities of finite aspect ratio (see Section 6). Applications to thermally driven flows in shallow cavities were previously discussed in Haruta [14]. Although the computational accuracy of these earlier results was lower than that of the present calculations, verification of the limit defined by (6.10) for the eddy structure in shallow cavities was clearly established.

Acknowledgement—The authors would like to thank Dr B. T. Murray, Dr P. G. Simpkins, and Professor E. Varley for numerous helpful discussions. This work was partially supported by NASA/LeRC under contract NAG3-1632.

REFERENCES

[1] L. PRANDTL, *Int. Congr. Math. (Heidelberg)*, p. 484 (1904).
[2] G. K. BATCHELOR, *J. Fluid Mechanics* **1,** 177 (1956).
[3] J. H. B. SMITH, *A. Rev. Fluid. Mech.* **18,** 221 (1986).
[4] D. W. MOORE, P. G. SAFFMAN and S. TANVEER, *Phys. Fluids* **31,** 978 (1988).
[5] S. WEINBAUM, *J. Fluid Mech.* **18,** 409 (1964).
[6] O. R. BURGGRAF, *J. Fluid Mech.* **24,** 113 (1966).
[7] R. GRIMSHAW, *J. Fluid Mech.* **39,** 695 (1969).
[8] A. E. GILL, *J. Fluid Mech.* **26,** 515 (1966).
[9] P. L. READ, P. B. RHINES and A. A. WHITE, *J. Atmos. Sci.* **43,** 3226 (1986).
[10] A. J. MESTEL, *J. Fluid Mech.* **200,** 1 (1989).
[11] A. T. PATERA, *J. Comp. Phys.* **54,** 468 (1984).
[12] Nekton v2.85 User's Guide, (1992).
[13] A. LIAKOPOULOS, Fifth Annual Forum on Unsteady Flow, ASME, (1988).
[14] E. HARUTA, Natural convection in a shallow cavity. M.S. thesis, Lehigh University (1989).

(Received 25 January 1995; accepted 2 March 1995)